ARTICLES
https://doi.org/10.1038/s41477-021-00981-3

nature plants

Check for updates

Live single-cell transcriptional dynamics via RNA labelling during the phosphate response in plants

Sahar Hani[1,11], Laura Cuyas[1,2,11], Pascale David[1,11], David Secco[3], James Whelan[3], Marie-Christine Thibaud[1], Rémy Merret[4], Florian Mueller[5], Nathalie Pochon[1], Hélène Javot[1], Orestis Faklaris[6], Eric Maréchal[7], Edouard Bertrand[8,9,10] ✉ and Laurent Nussaume[1] ✉

Plants are constantly adapting to ambient fluctuations through spatial and temporal transcriptional responses. Here, we implemented the latest-generation RNA imaging system and combined it with microfluidics to visualize transcriptional regulation in living *Arabidopsis* plants. This enabled quantitative measurements of the transcriptional activity of single loci in single cells, in real time and under changing environmental conditions. Using phosphate-responsive genes as a model, we found that active genes displayed high transcription initiation rates (one initiation event every ~3 s) and frequently clustered together in endoreplicated cells. We observed gene bursting and large allelic differences in single cells, revealing that at steady state, intrinsic noise dominated extrinsic variations. Moreover, we established that transcriptional repression triggered in roots by phosphate, a crucial macronutrient limiting plant development, occurred with unexpectedly fast kinetics (on the order of minutes) and striking heterogeneity between neighbouring cells. Access to single-cell RNA polymerase II dynamics in live plants will benefit future studies of signalling processes.

Plants are sessile organisms permanently coping with environmental variations. Transcriptional reprogramming[1] plays a key role in these responses as illustrated by the number of plant transcription factors (5.4% of proteins in *Arabidopsis*, https://agris-knowledgebase.org/). Most physiological studies quantify mRNA abundance in organs. Accessing specific cell types is possible by expressing a fluorescent marker in cells of interest to sort them and perform sequencing analysis[2]. Nevertheless, this requires long enzymatic digestion to generate protoplasts, preventing fast kinetic studies. Transcriptional fusions between promoters and reporter genes such as GFP provide cellular resolution, but the time required to accumulate detectable levels of mature fluorophore (often in the range of tens of minutes[3]) prevents rapid transcriptional monitoring. This is moreover highly variable and depends on the strength of the promoter studied and the microscopy setup, leading to confounding effects. These considerations are even more crucial when studying transcriptional inhibition. The above-mentioned experiments provide access to total RNA (or protein), resulting from the balance between synthesis and degradation. Many fluorescent proteins decay in the range of hours, and RNA degradation is highly variable from one gene to another[4,5]. For instance, the median half-life value of *Arabidopsis* mRNAs is 107 min, but it exceeds one day for many messengers[4]. This is far too long for transcriptional responses occurring within seconds, such as during light stress[6].

All these issues can be resolved with a method originally developed for yeast and animals that grants direct real-time access to transcriptional activity at the level of single cells[7–10]. It is based on a fusion between GFP and the bacteriophage MS2 coat protein (MCP–GFP)[7,8] or on related systems[11]. MCP–GFP recognizes a specific RNA stem–loop inserted in multiple copies into a reporter RNA, promoting MCP–GFP multimerization to provide a signal bright enough for single-RNA visualization[9]. Importantly, binding occurs during RNA synthesis and monitors transcription in real time. In plants, this technology would offer major advantages for physiological studies such as adaptations to biotic and abiotic stresses. Indeed, it grants access to the variability of all cell types, providing ways to understand how the activity of single cells is integrated within tissues or organs and thus to better understand gene regulation. Real-time quantitative analysis can be performed for transcription initiation, elongation or gene bursting. This last phenomenon can further be used to identify promoter states that are rate-limiting for transcription initiation and are thus likely points of regulation[12]. The MS2 technology also allows the identification of extrinsic and intrinsic sources of transcriptional noise.

We therefore implemented it in plants using state-of-the-art MS2×128 repeats to tag a single RNA with ~250 to 500 GFPs for optimal detection sensitivity[13]. We used this system to analyse the transcriptional response to a major macronutrient: inorganic phosphate (P_i). P_i deficiency triggers major transcriptional modifications affecting plant development and metabolism[14,15]. These are mainly controlled by master regulator genes of the PHR1 family[15–17]. Being constitutive, their regulatory activity relies on inhibitors of the SPX family tuned by P_i uptake[18,19], as they inhibit PHR1 activity only in the presence of P_i metabolites[20,21].

Here we used the promoters of early P_i responding genes to drive transcription of an MS2×128 reporter. We combined fast

[1]Aix Marseille Univ, CEA, CNRS, BIAM, UMR7265, SAVE (Signalisation pour l'Adaptation des Végétaux à leur Environnement), Saint-Paul lez Durance, France. [2]Agroinnovation International-TIMAC AGRO, Groupe Roullier, Saint-Malo, France. [3]Department of Animal, Plant and Soil Sciences, Australian Research Council Centre of Excellence in Plant Energy Biology, School of Life Sciences, La Trobe University, Bundoora, Victoria, Australia. [4]UMR5096 CNRS/Université de Perpignan, Laboratoire Génome et Développement des Plantes, Perpignan, France. [5]Unité Imagerie et Modélisation, Institut Pasteur and CNRS UMR 3691, Paris, France. [6]MRI, BioCampus Montpellier, CRBM, Univ. Montpellier, CNRS, Montpellier, France. [7]UMR 5168 CNRS-CEA-INRA-Université Grenoble Alpes, Laboratoire de Physiologie Cellulaire et Végétale, iRIG, CEA-Grenoble, Grenoble, France. [8]Institut de Génétique Moléculaire de Montpellier, Univ. Montpellier, CNRS, Montpellier, France. [9]Institut de Génétique Humaine, Univ. Montpellier, CNRS, Montpellier, France. [10]Equipe labélisée Ligue Nationale Contre le Cancer, Montpellier, France. [11]These authors contributed equally: Sahar Hani, Laura Cuyas, Pascale David. ✉e-mail: edouard.bertrand@igh.cnrs.fr; lnussaume@cea.fr

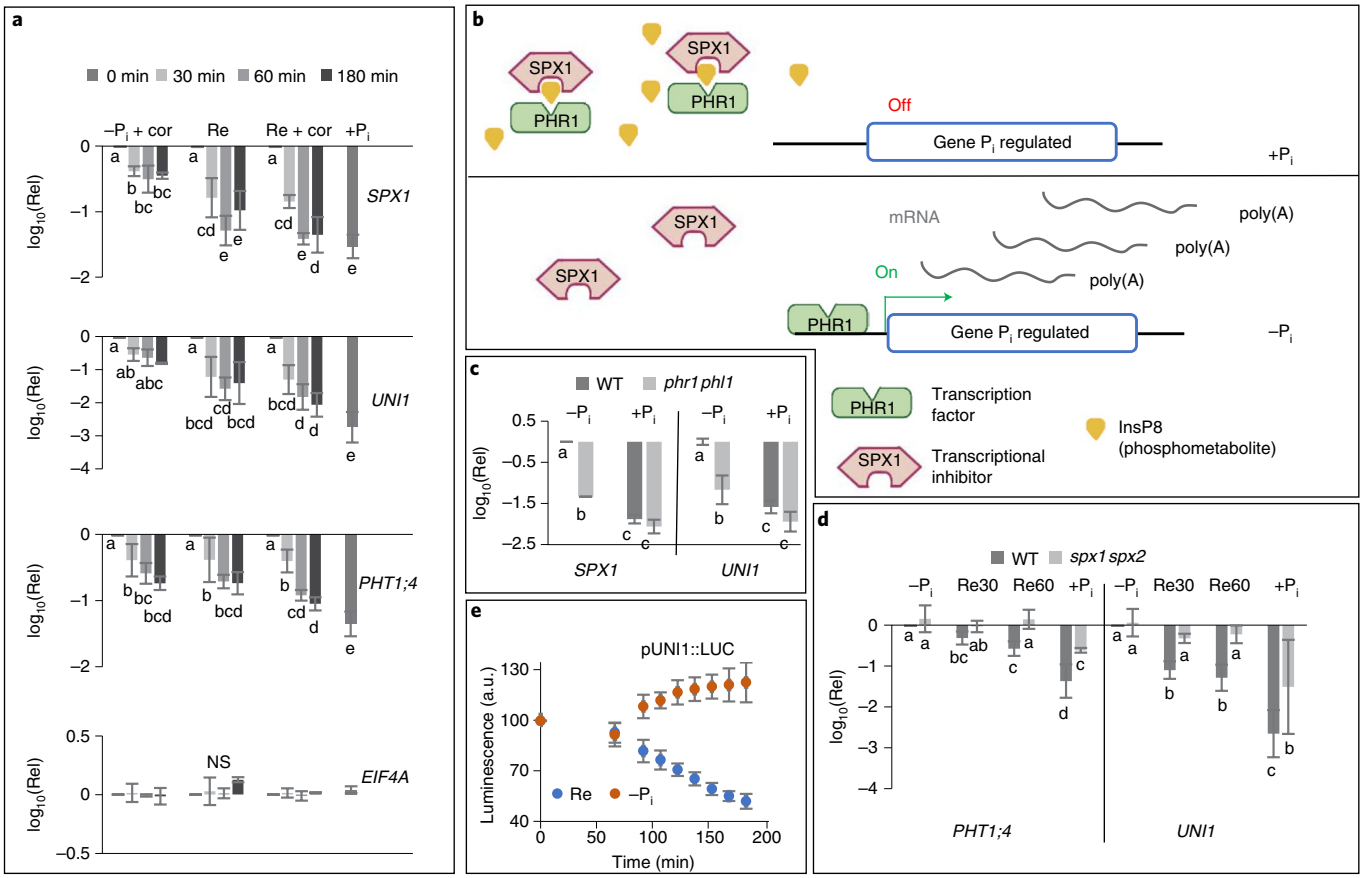

Fig. 1 | Identification of fast responsive transcripts regulated at the transcriptional level by phosphate resupply. a, RT-qPCRs of roots of seedlings grown for seven days in the presence of phosphate (+P_i), in the absence of phosphate (−P_i) or in the absence of phosphate for seven days followed by phosphate resupply (Re) for 30 minutes (Re30) or 60 minutes (Re60). *EIF4A*, a translation initiation factor known not to react to cordycepin (cor) addition, was used as a control[46]; $n = 2$–3. NS, not significant. **b**, Model depicting the transcriptional regulation by phosphate. **c**, RT-qPCRs of roots of wild-type (WT) and *phr1 phl1* seedlings grown for seven days under +P_i and −P_i; $n = 2$–3. **d**, RT-qPCRs of roots of WT and *spx1 spx2* seedlings grown for seven days under +P_i or −P_i and supplemented with P_i for 30 or 60 minutes; $n = 3$–5. **e**, Kinetics of luminescence measurements in pUNI1::LUC transgenic seedlings between −P_i and resupplied samples. The values are relative to −P_i; $n = 5$. a.u., arbitrary units. For all RT-qPCR experiments, *TUBULIN* was used as a housekeeping reference gene for normalization. The values are $\log_{10}$ relative expression levels (Rel) normalized to 1 for −P_i levels at time zero represented. Different letters indicate significantly different means (Student–Newman–Keuls one-way analysis of variance, $P < 0.05$, RStudio). The error bars represent standard deviations, and n is the number of biological replicates used for RNA extraction.

quantitative imaging and microfluidics[22] to precisely control P_i delivery while providing stable environmental conditions. This revealed a high heterogeneity of responses between adjacent cells and identified the rapid perception of P_i by the root (within 3–5 min), validating the power of the MS2 technology to dissect plant transcriptional regulation.

Results

Phosphate resupply promotes rapid transcriptional modifications. To identify early markers sensitive to phosphate, we starved plants and performed P_i refeeding experiments. After the addition of P_i in the liquid culture medium, we harvested roots and leaves after 30, 60 and 180 min for RNA-seq analysis. In roots, only 22 genes exhibited a significant twofold reduction in their transcript level over the three time points (Supplementary Fig. 1a,b). Analysis of the shoot samples revealed a delayed reduction of all these markers in aerial parts (only one-third were repressed after 30 min), indicating that P_i was first perceived by roots. Independent experiments analysed by quantitative PCR with reverse transcription (RT–qPCR) using well-known markers for P_i starvation[15,23], involved in P_i uptake (*PHT1;4*) or P_i-induced metabolic remodelling (*SQD2*), confirmed these results (Fig. 1a and Supplementary Fig. 1b). The rapid downregulation observed also highlighted the fast turnover of these transcripts (half-life estimated to be 15–30 minutes; Supplementary Fig. 1a,b) relative to the *Arabidopsis* median value of 3.8 hours[5]. For the rest of this study, we selected two genes (*SPX1* and At5G20790, named hereafter *UNI1* for *Unicorn1*), which combined the highest levels of expression in P_i-depleted medium (−P_i) with broad dynamics as measured by +P_i/−P_i fold change.

Regulation was assumed to occur mainly transcriptionally, as the transcriptional inhibitor cordycepin mimicked the effect of P_i resupply (Fig. 1a). This was confirmed by transcriptional fusions with luciferase, which conferred to the reporter gene a similar temporal response to P_i resupply (Supplementary Fig. 1c), whereas fusing a CaMV 35S constitutive promoter to the coding region of the markers did not reveal any significant difference in RNA levels between +P_i (after 180 min of refeeding) and −P_i conditions (Supplementary Fig. 1d), except for short transient induction promoted by the stress of P_i addition observed during the first hour following resupply. A sequence analysis of the 22 genes identified above revealed the presence of P1BS regulatory boxes[16] in 95% of the cases. This box is the binding site of master regulators belonging to the PHR1/PHL1 family. The addition of P_i promotes the synthesis of inositol pyrophosphates, which act as molecular tethers to fix members of the SPX

family to PHR1 and inhibit its activity[20,21] (Fig. 1b). Consistently, the induction of *SPX1* and *UNI1* during P_i starvation was nearly fully abolished in *phr1 phl1* double mutants, which suppress a majority of PHR1/PHL proteins (Fig. 1c). Moreover, this was observed for 91% of the 22 genes identified (Supplementary Fig. 1a; see also ref. [17]). SPX family members inhibit PHR1, and the analysis of *spx1 spx2* double mutants further revealed that reducing the SPX protein pool delayed the repression triggered by P_i addition (Fig. 1d). Altogether, these results demonstrated that the fast decrease of the 22 transcripts identified here resulted from transcriptional control involving several key players such as the PHR and SPX families of proteins. Of note, classical transcriptional fusion with luciferase did not result in a fast transcriptional repression (Fig. 1e). More than one hour was required to observe a notable decrease in the signal, whereas RT–qPCR failed to detect a significant reduction of mRNA levels for at least 15–20 minutes after resupply (data not shown). To better characterize the transcriptional response to P_i resupply, we implemented the MS2 system for RNA labelling, a technology so far restricted mostly to animal and yeast cells but offering unique spatio-temporal resolution to study transcriptional regulation.

Generation and validation of MS2-tagged *Arabidopsis* lines. We used the last-generation MS2 tag containing 128×MS2 repeats, originally developed to image single molecules of HIV-1 RNA[13]. To improve RNA folding and prevent plasmid instability, this construct is made of 32 distinct MS2 stem–loops replicated four times, with each stem–loop binding dimers of the MCP protein with sub-nanomolar affinity[13] (Fig. 2a). In animal cells, this extended tag provides about a fivefold improved sensitivity over the original MS2×24 tag and allows single-molecule visualization for extended periods even at high frame rates[13]. Moreover, this construct bears the lower-affinity variant of the MS2 stem–loops (U instead of C in the third position of the loop), providing excellent RNA visualization while preserving normal RNA degradation[24].

We developed Moclo vectors adapted to the Golden Gate system[25] to facilitate the cloning and use of the MS2×128 recombinogenic sequence (Supplementary Fig. 2a), and we generated transcriptional fusions with the *SPX1* and *UNI1* promoters (Fig. 2a). We then introduced into the binary vector used for plant transformation a gene expressing a nuclear targeted MCP–eGFP fusion protein[13] under the control of the weak constitutive Ubiquitin-10 promoter[26] (Supplementary Fig. 2a). For the two constructs, genetic analysis selected homozygous transformants exhibiting single-locus insertions. We first focused on the homozygous pSPX1::MS2×128 line named 'S' for 'strong' and exhibiting the best signals. Molecular analysis revealed the insertion of three copies of the transgene at a single locus in the S line (Supplementary Fig. 3). The presence of the cap and the poly(A) tail, crucial elements for RNA stability, was also verified for MS2×128 transcripts (Supplementary Fig. 4). Single-molecule fluorescence in situ hybridization (smFISH) was performed on root squashing to analyse the phosphate response of the transgenes. Root squashing allows good probe penetration in tissues and causes some cells to fall off the root and adhere to coverslips as a monolayer[27], allowing high-quality imaging using wide-field microscopy with high numerical aperture objectives (Fig. 2b and Supplementary Fig. 2b). The fluorescent oligonucleotide probes hybridizing against the MS2 stem–loops labelled the reporter RNA in most tissues of the root grown on P_i-depleted medium, including the root cap and mature tissues (Figs. 2b and 3), and they did not detect signals in Col-0 negative controls lacking the transgene (Supplementary Fig. 5). Interestingly, the smFISH signals were rarely detected in the cytosol and mostly stained nuclei, where transcription sites were visible as bright spots. This nuclear localization could be due to either a nuclear retention of the MS2-labelled RNA or a reduced stability in the cytosol. In any case, the smFISH signal disappeared when plants were grown in the presence of phosphate (Fig. 2b, right panels). Quantification of the signals indicated that 74% of the cells expressed the pSPX1::MS2×128 transgene in the absence of phosphate (>20 RNA per cell), and none in its presence (Fig. 2c,d). To further validate these results, we visualized the endogenous *SPX1* transcripts with a mix of 24 fluorescent oligonucleotide probes specific to SPX1. In P_i-depleted conditions, the probes identified the transcription sites and single mRNA molecules present in the cytoplasm, as expected for a translated transcript (Fig. 2c and Supplementary Fig. 2b). Similar to the pSPX1::MS2×128 reporter, the endogenous *SPX1* mRNA was expressed throughout the root, including the cap and mature tissues[28], with a number of positive cells similar to that of the reporter (Fig. 2d). Importantly, *SPX1* smFISH signals were very low in plants growing on P_i-rich medium (Fig. 2c,d, right panels) and completely absent in a *spx1 spx2* double mutant used as a negative control (Supplementary Fig. 6). Overall, these data indicated that the MS2 transgene driven by the *SPX1* promoter faithfully reported on the expression of *SPX1*, with a similar regulation and spatial expression pattern.

Imaging transcription in fixed tissues of whole plants with MCP–GFP. We then turned to spinning disk confocal microscopy to image plants through the tissue depth (reaching 100 µm) and to assess in detail the performance of MCP–GFP in imaging transcription. We first used the brightest homozygous pSPX1::MS2×128 line (called S) to image the expression of the reporter in the root (Fig. 3a; a viewer with a zoomable high-resolution image can be accessed at https://imjoy.io/lite?plugin=muellerflorian/hani-ms2:hani-ms2-sample-3 and https://imjoy.io/lite?plugin=muellerflorian/hani-ms2:hani-ms2-sample-1), which is a continuously growing organ with a well-defined architecture. At the apex, the root cap encapsulates the meristematic zone, where cells divide rapidly until they enter the transition zone. Cells then elongate and initiate tissue differentiation according to a well-defined radial pattern, generating a number of different cell types (Fig. 3a).

First, we tested whether MCP–GFP could faithfully report on the MS2-tagged RNA, and we performed smFISH together with MCP–GFP imaging. In the root cap, which is mostly composed of diploid cells[29], smFISH against the MS2 stem–loops revealed both

Fig. 2 | Validation of pSPX1::MS2×128 transgenic plants. a, Principle of the MS2–MCP system. The transgene is under the control of the *SPX1* promoter and synthesizes a reporter RNA bearing 128 MS2 stem–loops, which are recognized by the MCP protein fused to a fluorescent marker (eGFP). **b**, Microscopy images of squashed root caps of the transgenic S line expressing pSPX1::MS2×128 and processed for smFISH with probes hybridizing to the MS2×128 sequence. Left, P_i-depleted sample ($-P_i$) and zoomed over the boxed area in the middle panels. Right, sample grown on P_i-rich medium ($+P_i$). Top, smFISH signals; bottom, smFISH signals coloured in red and merged with 4,6-diamidino-2-phenylindole (DAPI) (blue). The images are maximal projections of *z*-stacks (widefield microscopy). Scale bars, 40 µm (left and right panels) and 4 µm (middle panels). Transcription sites and single RNA molecules are indicated by orange and pink arrows, respectively. **c**, Legend as in **b** except that smFISH was performed with probes hybridizing against the endogenous *SPX1* mRNAs in WT squashed roots in the cap (right) and mature tissue (left). Scale bars, 4 µm. **d**, Bar plot depicting the number of cells expressing the endogenous *SPX1* mRNA (orange, WT plants) or the pSPX1::MS2×128 reporter RNA (blue, S plants) in roots (the data for root cap and mature root area are combined), with ($+P_i$) or without ($-P_i$) phosphate. The mean and standard deviation are estimated from 12 fields of view for the *SPX1* probes ($n = 300$) and 23 for the MS2 probes ($n = 3{,}087$). Expressing cells are defined here as cells having at least 20 RNA molecules in the nucleus or the cytoplasm.

single molecules and transcription sites, visible as bright spots in the nucleus (Fig. 3b, bottom panels; pink and orange arrows, respectively). In both root cap (Fig. 3b) and mature tissue (Fig. 3c), we observed colocalization between the smFISH signals revealed by MS2 probes and the fluorescent signals produced by MCP–GFP. The transcription sites were easily detected (Fig. 3b,c, orange arrows), and MCP–GFP could also reveal the putative brightest single mRNAs (Fig. 3b, pink arrows). To assess the reliability of

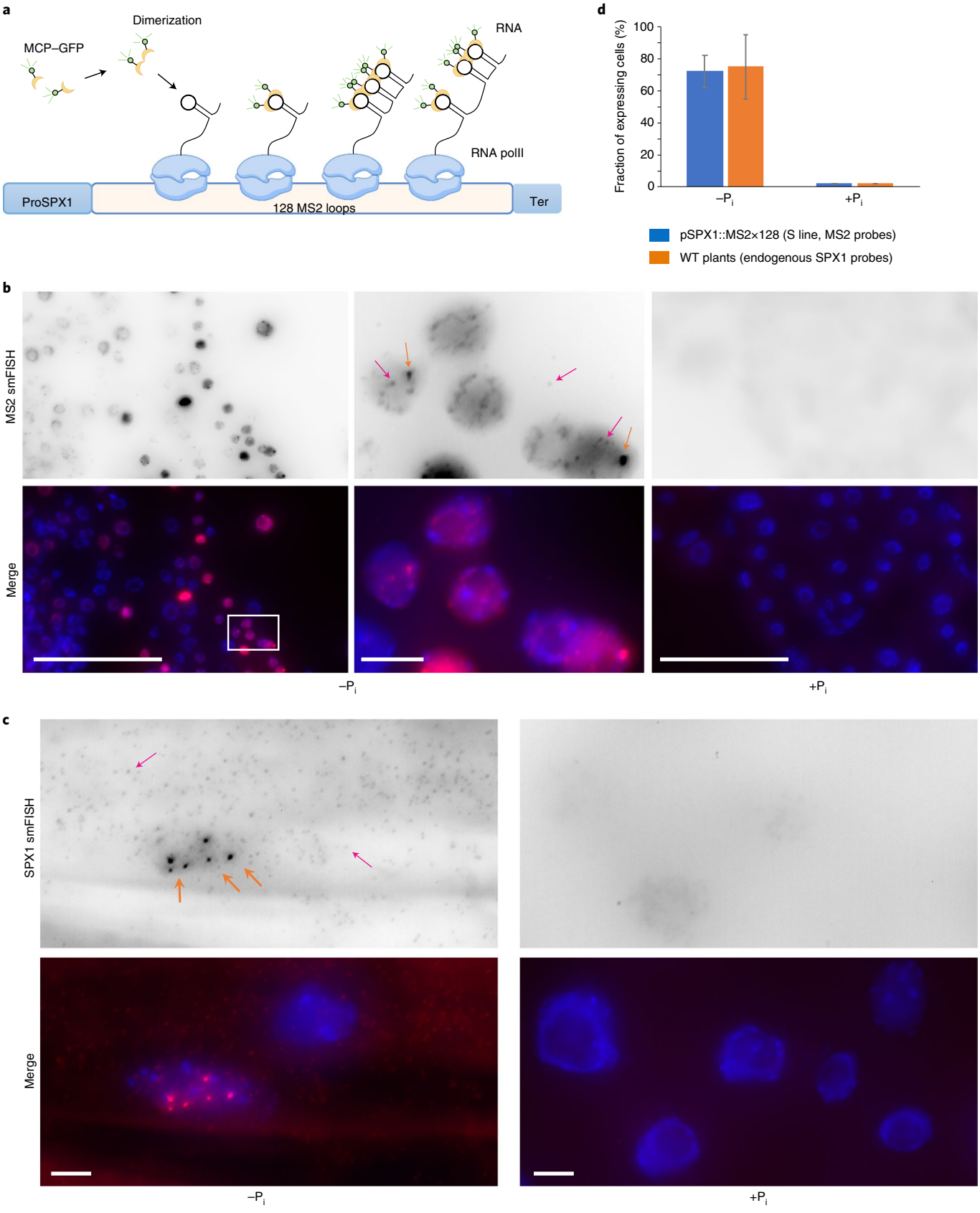

detection, we counted transcription sites in both colours and found that 90–95% of the sites detected by MCP–GFP were also labelled by MS2 smFISH.

Finally, we extended these observations to other *Arabidopsis* lines, using plants having either the pUnicorn1::MS2×128 reporter or another single-locus transformant of the pSPX1::MS2×128 transgene (J line). The J line turned out to also present multiple transfer DNA copies (Supplementary Fig. 3b), but it exhibited reduced levels of fluorescence when compared with the S line. The transcription sites of the reporters were readily detected with MCP–GFP and colocalized with the MS2 smFISH signals (Supplementary Fig. 7). Overall, these results validated the MS2–MCP system as a robust and sensitive system to image transcription in whole plant tissues.

Single-molecule counting by smFISH gives insights into the dynamics of transcription in *Arabidopsis thaliana*. The ability of smFISH to detect single RNAs enables a quantitative analysis of the RNA polymerase II transcription cycle[9,12,30,31]. We therefore measured the brightness of transcription sites and used the visible single molecules to compute the absolute number of nascent RNA molecules at active transcription sites (Fig. 4a,b and Methods). We obtained an average of 37 molecules at the transcription site of the pSPX1::MS2×128 reporter for the S lines, with a main peak at ~20 molecules (Fig. 4a). We also designed a set of 21 fluorescent oligonucleotides against the sequence immediately downstream of the polyadenylation site of the reporter (Supplementary Fig. 12). However, we failed to detect any smFISH signal, indicating that 3′-end processing was more rapid than transcription. This agrees with previous GRO-seq experiments that revealed that RNA polymerases terminate transcription very rapidly after poly(A) sites[32,33]. We repeated these measurements for the endogenous *SPX1* mRNA and found an average of 11.3 molecules at transcription sites, with a main peak at 9 molecules. Given that the *SPX1* gene is 1.4 kilobases (kb) long, this number suggests that active *SPX1* genes have one polymerase every 77 bases if 3′-end processing is immediate, and one polymerase every 120 bases if 3′-end processing takes a minute[13] (assuming an elongation rate of 2 kb min^{-1}; ref. [30]). For the 3 kb pSPX1::MS2×128 reporter, similar numbers were found if one considers that the peak of 25 molecules at a transcription site corresponds to a single active copy (Fig. 4a). These numbers indicate that active *SPX1* genes have an initiation event every 2.3 to 3.5 seconds on average (Methods and the schematic in Fig. 4b). This is in the high range of previous estimates obtained in human cells and *Drosophila*[13]. It suggests that transcription in *Arabidopsis* is rapid and occurs in the form of polymerase convoys, produced by initiation events rapidly occurring one after another when the gene turns on[13].

Quantitation of *SPX1* transcription in fixed roots reveals cell polyploidy in mature tissue as well as large allelic differences. Endoreplication occurs frequently in root with DNA cell contents ranging from 2C to 16C (ref. [29]). This phenomenon increases as one moves away from the root tip. Being involved in the size of the cells, it also varies and increases from the central to the expanded external cell layers such as cortex or epidermis[29] (Fig. 3a). The number of transcription sites present in each nucleus highlighted this endoreplication. In the root apex of the pSPX1::MS2×128 S line, cells of the columella (extremity of the root cap) exhibited no more than two transcription sites for the MS2 reporter or the endogenous *SPX1* gene in the vast majority of cases, as expected for a mainly diploid tissue[29] (Figs. 3b and 4c for quantifications). In contrast, images recorded in the differentiated part of the root revealed the more complex nature of older tissues with the presence of cells with many transcription sites, indicating polyploidy (Figs. 2c and 3c). Quantification of the number of active alleles per cell indicated that in diploid columella cells, only 3% of the cells had more than two transcription sites, while in the mature tissue, 35% had more than two sites, with 2% having as many as seven (Fig. 4c,d). Similar numbers were obtained with the endogenous *SPX1* gene (Fig. 4d). Interestingly, we noted that in cells with many active alleles, the *SPX1* transcription sites frequently clustered in the nucleoplasm, most often forming two groups (see Fig. 4f for an example). To explore this further, we measured the distance between all visible transcription sites in cells having four to eight active sites, and we compared the resulting distance distribution with a situation where we simulated eight sites with random locations (Fig. 4e and Methods). This showed that the transcription sites had a non-random distribution and were frequently close to one another, with 40% of the distances falling within 1.5 µm. This phenomenon was also visible when we compared the brightness of transcription sites in cells having one or two transcription sites with that in cells having four or more sites (Supplementary Fig. 2c). Cells with one or two SPX1 transcription sites had a single peak at 10 nascent RNAs, while cells with four or more sites had a second peak at 20 nascent RNAs (Supplementary Fig. 2c). This suggests that in these cells, some transcription sites had coalesced into a single spot, reminiscent of the 'transcription factories' previously described in human cells[34].

Next, we compared the activities of the different alleles of single cells, focusing first on diploid root cap cells. Surprisingly, a substantial number of cells exhibited only a single active transcription site (30% of the cells; Fig. 4c) or no transcription at all (39%). This was also observed with the endogenous *SPX1* gene (Fig. 4d), indicating that it is a feature of this *Arabidopsis* gene and not an artefact of the MS2 reporter. Since the cells with no transcription sites contained smFISH signal in the nucleoplasm or the cytoplasm (Fig. 3), transcription had been active in these cells, therefore indicating that *SPX1* promoter activity was discontinuous. Such discontinuous transcription is the result of gene bursting and has been observed in many organisms, including yeast, *Drosophila* and mammals[35]. To our knowledge, it has not been reported so far in plants. Gene bursting involves the stochastic switching of a promoter between active and inactive states. It depends on mechanistic aspects of transcription initiation as well as transcriptional regulation[12]. This stochasticity causes variations in gene expression among identical cells (that is, gene expression noise), which sometimes has important phenotypic consequences[12]. Commonly, two sources of noise are distinguished: intrinsic and extrinsic. Intrinsic noise is due to the stochastic nature of biochemical reactions involving a single molecule of DNA and the transcription factors acting on it, and it occurs independently on each allele. In contrast, extrinsic noise

Fig. 3 | Imaging of *SPX1* transcription in fixed plant tissues reveals allelic differences in the root cap and polyploid expression in mature tissue. **a**, Organization of *Arabidopsis* root, with the names of the various root parts and tissues overlayed on a microscopy mosaic image of a homozygous S plant with MCP–GFP (green) and DNA (blue). Inset: ploidy of the root tissue. Note that a viewer with a zoomable high-resolution version of the mosaic can be accessed at https://imjoy.io/lite?plugin=muellerflorian/hani-ms2:hani-ms2-sample-3. **b**, Images are maximal image projections (MIPs) of a *z*-stack from a root cap of a homozygous S plant grown without P_i and imaged by spinning disk microscopy in three colours. Left (and red in the merged panel), smFISH signals obtained with probes against the MS2 repeat; middle (and green in the merged panel), MCP–GFP signals. Blue indicates nuclei stained with DAPI. The bottom panels are zooms of the boxed area in the merged panel. The pink arrows indicate single RNA molecule, and the orange arrows indicate transcription sites. Scale bars, 100 µm (top panels) and 10 µm (bottom panels). **c**, Legend as in **b**, except that a mature part of the root is imaged. Note that the images in **a**, **b** and **c** come from different plantlets.

modulates both alleles similarly as the result of events affecting the entire cell (such as cell cycle or the activation of a signalling pathway). Interestingly, our capability of accessing several alleles within a cell raised the possibility of discriminating between the two causes of transcriptional noise. For each cell that had only one or two active alleles, we plotted the brightness of one *SPX1* allele as a function

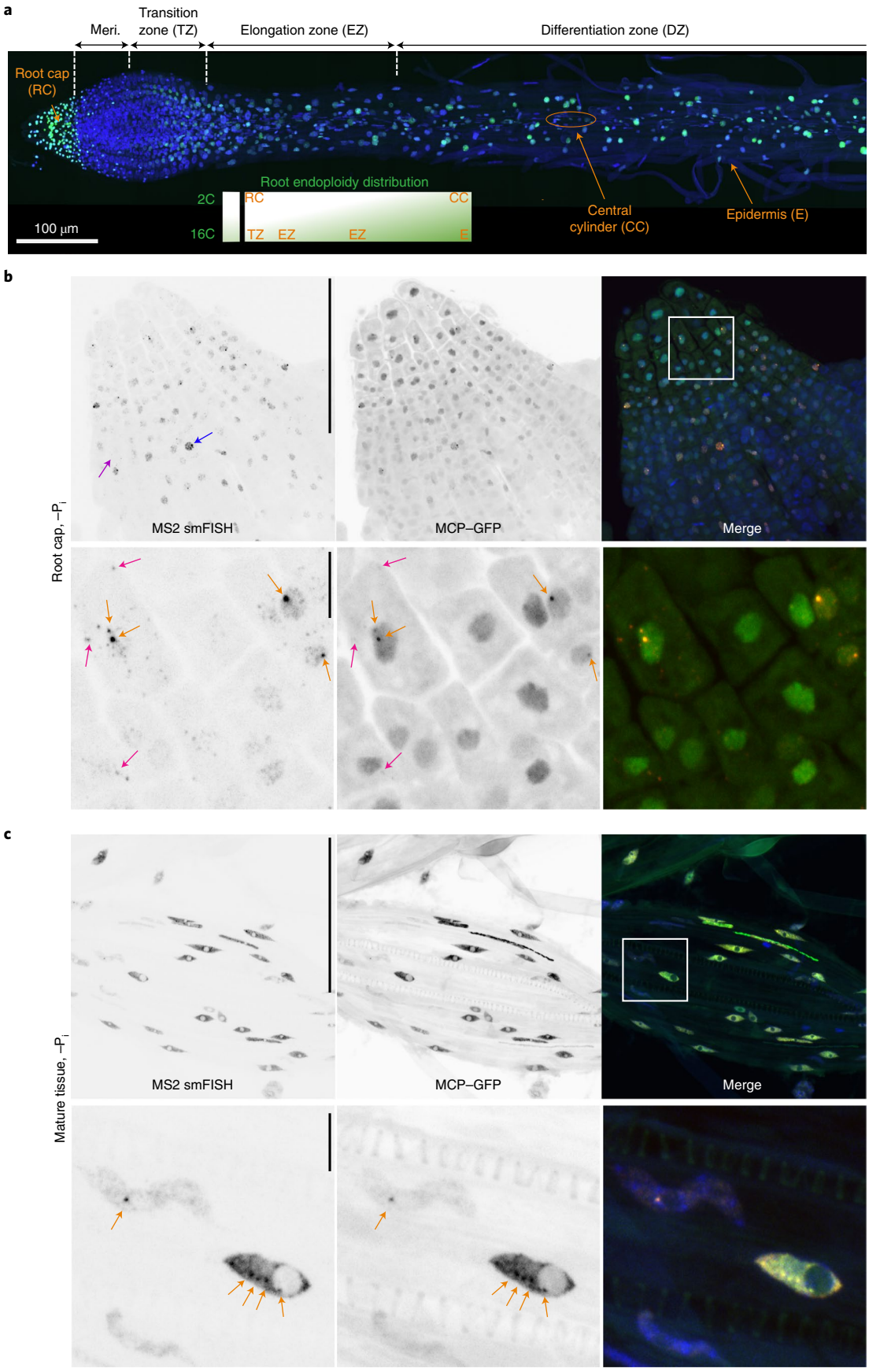

of the other (Fig. 4g). This revealed both correlated (cells on the diagonal) and uncorrelated (cells off the diagonal) transcriptional activities of these alleles. To quantify this phenomenon further, we measured the total, intrinsic and extrinsic noise[36,37], using cells having either exactly two active transcription sites or three or four such sites (Fig. 4h and Methods). As expected from the results described above, we found that the total noise had important intrinsic and extrinsic contributions, with intrinsic noise being the dominant source. This highlights the quantitative importance of transcriptional noise for *Arabidopsis*.

Real-time visualization of *SPX1* transcription reveals gene bursting and P_i-mediated repression. We used a simplified version[38] of the RootChip microfluidic system[22] to combine live-cell imaging with the capacity to change the phosphate solution rapidly (Fig. 5a and Supplementary Videos 1–8). Imaging was performed with spinning disk microscopy, which offered the best compromise between image quality, size of the field of view and image acquisition speed. A typical experiment recorded at each time point a *z*-stack of 200 images with a *z*-spacing of 500 nm, allowing us to image at high resolution the entire root and thus access all its tissues. One image stack was recorded every two to three minutes for about one hour, and maximum intensity projection produced clear images where multiple transcription sites could be analysed. Using the brightest S line expressing pSPX1::MS2×128 and grown without P_i, images from the first time point confirmed the transcriptional heterogeneity between cells, with neighbouring cells exhibiting zero, one, two or even more active transcription sites and with the intensity of transcription sites varying by a factor of four (Figs. 5–7 and Supplementary Videos 3–7). Observation of the root constantly supplied with $-P_i$ solution directly demonstrated bursting of the *SPX1* promoter, with transcription sites coming on and off over periods of minutes (Fig. 6 and Supplementary Videos 1 and 2). Interestingly, this phenomenon was observed mainly in the root cap and only very rarely in mature tissues. The arrest of transcription after a burst provided an opportunity to visualize the release of putative single RNAs from the transcription sites (Fig. 6d and Supplementary Video 2), highlighting the dynamics of the process and suggesting single-molecule sensitivity in live plants.

Next, we analysed the response to P_i resupply. To this end, the S line was first grown for a few days in $-P_i$ liquid medium before receiving phosphate-rich medium combined with SynaptoRed fluorescent dye. This allowed us to precisely record the arrival of the supplemented media on the imaging field, thereby defining the time 0 of the time course. The movement of nuclei in the cells and the displacement of cells themselves complicated transcription site tracking. To simplify the analysis of the time course, we therefore used only cells with one or two active transcription sites. The repression of transcription upon P_i resupply proved to be rapid (Figs. 5a–c and 7a,b, Supplementary Figs. 8 and 9 and Supplementary Videos 3–7). The signals were then normalized to the value obtained at time 0 (Fig. 7c), and an average response curve was produced (Fig. 7d). The measurements were repeated with independent samples, and they all showed similar curves with a signal starting to decrease between zero and six minutes after P_i provision at the root surface (Fig. 7e). Similar results were obtained with the independent transgenic J line (Supplementary Fig. 10 and Supplementary Video 8), revealing the extraordinary sensitivity and rapidity of the regulatory cascade triggered by P_i.

The decrease in fluorescence starting when P_i resupply reached the root continued until it reached a plateau 18 to 25 minutes later (Fig. 7f and Supplementary Fig. 10). Interestingly, cells presenting multiple transcription sites revealed on average a close coordination of the repression between these sites, indicating that extrinsic factors dominate gene regulation when P_i repression initiates, as expected for a signalling pathway affecting the entire cell (Figs. 5c and 7b and Supplementary Fig. 8). Controls continuously supplied with P_i-depleted solution in mature tissue did not show significant changes (Fig. 7g,h and Supplementary Fig. 11) over a 25 min observation period.

The comparison between the MS2 and RT–qPCR results revealed a delay of 20–30 minutes for the RT–qPCR to show the maximum repression, which is in agreement with the *SPX1* mRNA half-life previously estimated in the range of 15–20 min (Fig. 1a and Supplementary Fig. 1a,b). Overall, these results demonstrate the unexpectedly fast dynamics of the plant response to P_i resupply, and they illustrate the capacity of the MS2 system to access transcriptional regulation in live plants. It should be noted that in mature tissues, we restricted the analysis to nuclei exhibiting one or two active alleles to avoid misattribution during the analysis (resulting from nuclei movement during analysis). This favours the representation of more central cells (less affected by polyploidy), which are known to be less affected by P_i repression compared with cortex or epidermis cells[39]. This may explain the slight difference (around 10%) in the average extent of the decrease in expression between RT–qPCR and MS2 live imaging.

Discussion

Large MS2 arrays and microfluidics reveal single-cell transcriptional dynamics in live plants. Fluorescent RNA technologies provide access to single-molecule studies offering invaluable insights into gene expression mechanisms[12,40]. A previous attempt to use these technologies in plants studied a highly abundant viral RNA in transient transformants, and a low signal-to-noise ratio prevented their use in stable plant lines[41]. The MS2×128 construct developed here (which uses six times more MS2 loops) solves this problem and

Fig. 4 | Quantitation of *SPX1* transcription in fixed cells gives insights into transcription dynamics, ploidy and intrinsic versus extrinsic noise. a, Graph depicting the distribution of the brightness of active transcription sites for the endogenous *SPX1* gene (left) or the SPX1–MS2×128 reporter (right), both detected by smFISH. The brightness values are expressed in number of full-length RNA molecules (*x* axis), and the *y* axis represents the number of cells with these values. **b**, Model of *SPX1* transcription, based on smFISH data labelling the endogenous *SPX1* mRNAs. **c**, Graph depicting the number of active transcription sites per cell for the SPX1–MS2×128 reporter detected by smFISH on four plants (488 nuclei) for mature tissue and three plants (641 nuclei) for root cap. The *x* axis shows the number of active transcription sites per cell; the *y* axis shows the fraction of cells with these values. The orange bars indicate diploid root cap cells, and the blue bars indicate differentiated, polyploid cells. The error bars represent standard deviation. **d**, Graph depicting the number of active transcription sites per cell for the endogenous *SPX1* mRNA detected by smFISH on nine plants (300 nuclei) for mature and three plants (137 nuclei) for root cap. Legend as in **c**. **e**, Histogram depicting the distance distribution between active transcription sites in single cells for the endogenous *SPX1* gene and for polyploid cells having four or more sites. Distances are expressed in µm (*x* axis), and the *y* axis represents the number of cells with these values. The pink curve indicates the distance distribution obtained by simulating a random location of eight spots within *Arabidopsis* nuclei. **f**, Image is a MIP of a *z*-stack from a differentiated root cell labelled by smFISH with probes against the endogenous *SPX1* mRNA (wide-field microscopy). Red indicates smFISH signals; blue indicates nuclei stained with DAPI. Scale bar, 5 µm. **g**, Graph depicting the correlation of activities of *SPX1* alleles, in cells having one or two active transcription sites. The *x* axis shows the number of molecules at the first transcription site; the *y* axis shows the number of molecules at the second transcription site. **h**, Graph depicting the levels of total, intrinsic and extrinsic noise for cells with either two active transcription sites (left) or three or four (right). The error bars represent the error estimated by bootstrapping (Methods).

provides direct access to the transcriptional activities of live plants, at the level of single alleles and with a sensitivity nearing single RNAs. Nevertheless, single-molecule detection remains difficult and not exhaustive, due in particular to the necessity of limiting illumination power to prevent bleaching and phototoxicity when acquiring 200 *z* planes for tens of time points. We hope that new constructions currently underway, in which the number of MS2 loops is doubled (256) or MCP–GFP expression is optimized, will provide important future improvements. Originally developed for yeast or mammalian cell lines, fluorescent tagging of RNA has been introduced in only a few multicellular organisms (*Drosophila* embryos in particular[10,35]), mostly to study transcriptional regulation during embryonic development and in the absence of external perturbations. Here, the implementation of microfluidics allowed complete control of environmental conditions and the investigation of the root response to phosphate starvation and resupply. Measurements

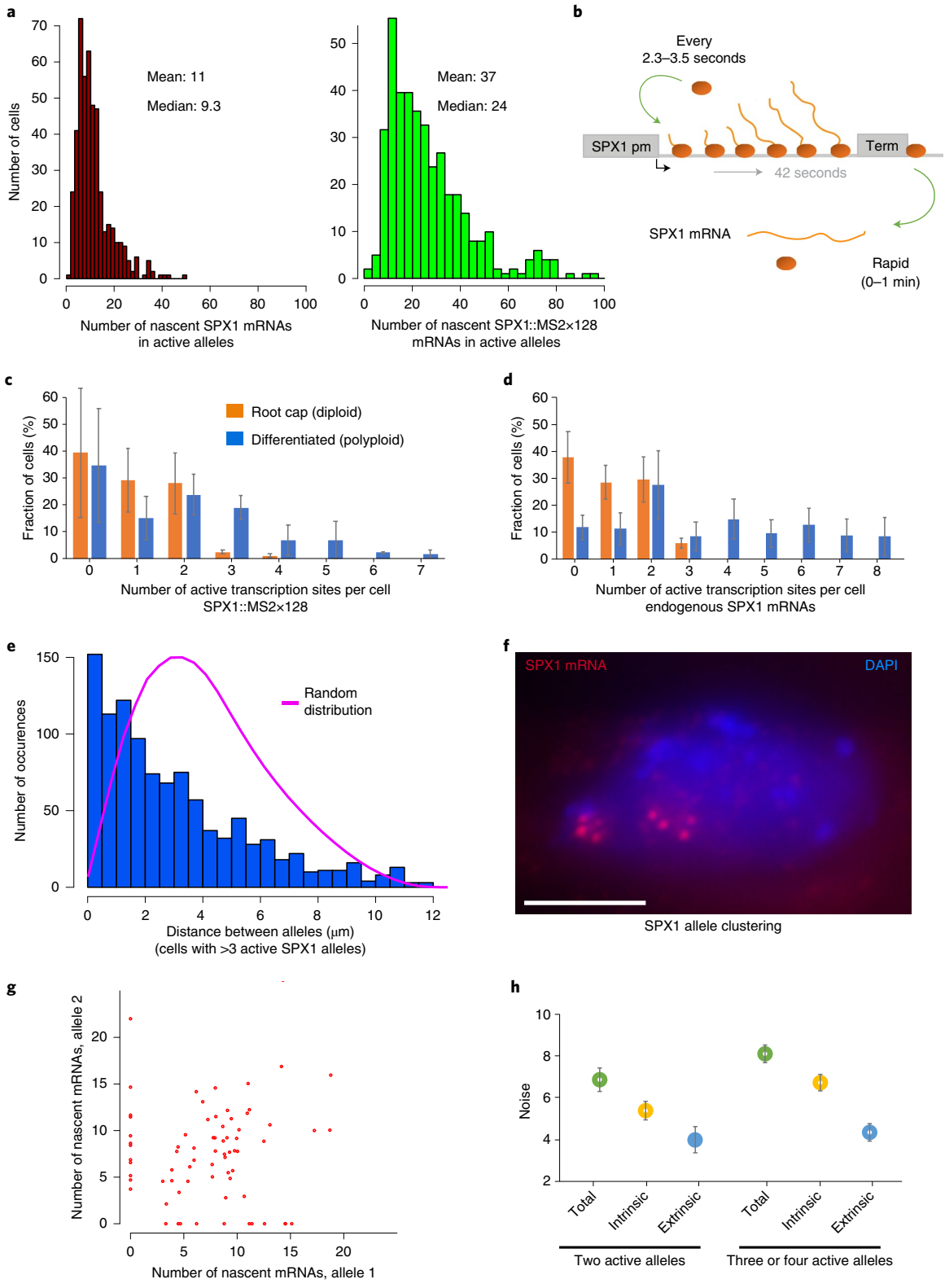

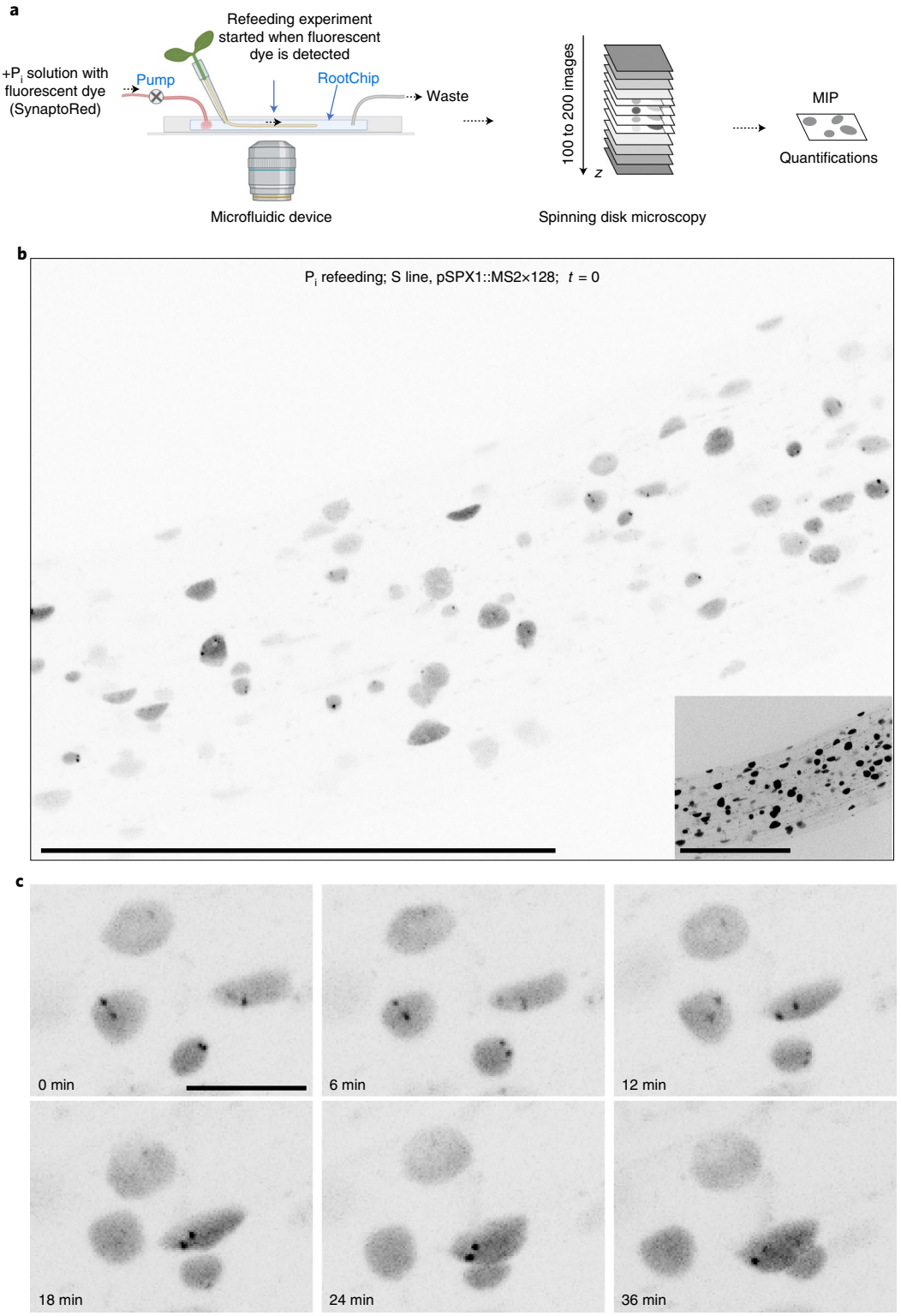

Fig. 5 | Combining microfluidic and MS2 technology reveals fast transcriptional repression triggered by P_i supply in pSPX1::MS2×128 transgenic plants. **a**, Schematic of the experiment combining the RootChip microfluidic system with spinning disk microscopy to analyse the transcriptional response to P_i refeeding in real time. **b**, Image is an MIP from a time-lapse video recorded in 3D (200 *z* planes), which displays MCP-GFP fluorescence in S plants at the start of P_i refeeding ($t = 0$). Scale bar, 100 µm. Inset: identical image with a higher contrast to display the tissue structure. **c**, Images are MIPs from the time-lapse video shown in **b**, taken at the indicated time points after P_i refeeding and displaying MCP-GFP fluorescence. Scale bar, 10 µm.

of transcriptional inhibition often suffer from indirect measurements introducing a considerable lag time in repression detection and from ensemble measurements averaging effects. In contrast, the tools developed here allow the visualization of repression in real time and single cells, and demonstrate that repression is a very rapid process that takes place in minutes.

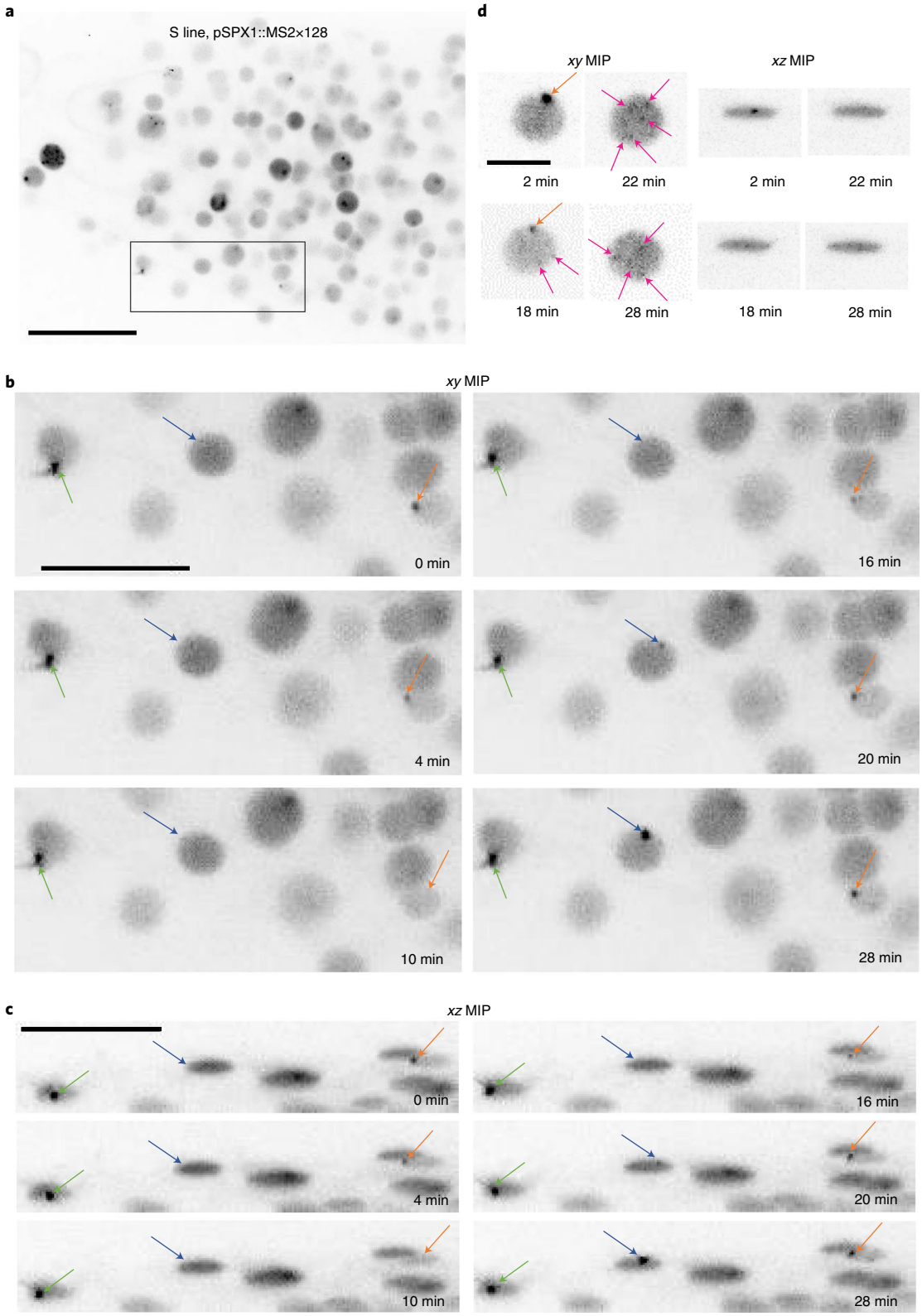

Fig. 6 | The *SPX1* promoter generates bursts of activity in root cap cells grown at steady state in the absence of phosphate. a, Image is an MIP from a time-lapse video recorded in 3D (44 *z* planes 600 nm apart), which displays MCP–GFP fluorescence in S plants. Scale bar, 20 µm. **b**,**c**, Images are MIPs on *xy* (**b**) or *xz* (**c**) axes from the time-lapse video shown in **a**, taken at the indicated time points and displaying MCP–GFP fluorescence. The arrows pinpoint transcription sites where the signal remains constant (green), increases (blue) or turns off and then on (orange) during the time lapse. Scale bars, 10 µm. **d**, Images are MIPs on *xy* (left) or *xz* (right) axes of a nucleus where transcription decreases at the transcription site (orange arrow) and individual mRNAs released can be seen (pink arrows). Scale bar, 5 µm.

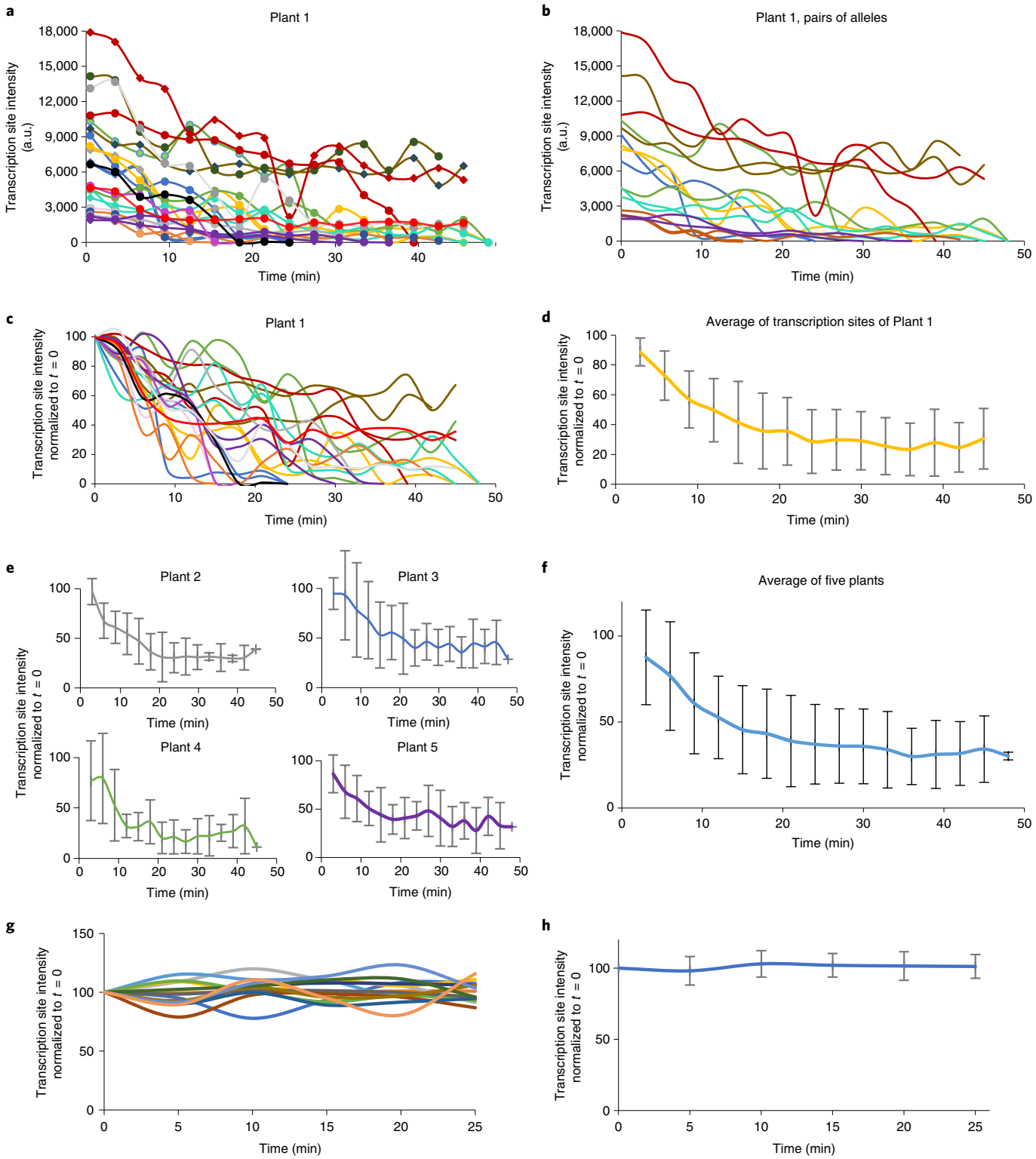

Fig. 7 | Analysis of transcription site activity following P_i supply in pSPX1::MS2×128 S line transgenic plants. a, Intensity of fluorescence signals at transcription sites in a.u., recorded every three minutes after P_i refeeding, for cells exhibiting one or two active transcription sites ($n = 22$) recorded in 14 mature root cells located 1 mm above the root tip. **b**, Intensity of fluorescence of transcription sites over time, for eight cells exhibiting two active transcription sites (plotted in the same colour). **c**, Normalized intensities of transcription sites over time, for the same cells as in **a**. The normalization was done according to the value measured at $t = 0$. **d**, Average normalized intensities of transcription sites, for the 22 transcription sites shown in **a** and **b** (mean and standard deviation). **e**, Same average curve of normalized transcription site intensities as in **d** obtained with independent plant samples. **f**, Average curve obtained by analysis of 67 transcription sites analysed in five plants. **g**, Intensity of fluorescence signals at transcription sites in a.u., recorded every three minutes for cells exhibiting one or two active transcription sites of plants supplied with P_i-depleted nutrient solution ($n = 14$). **h**, Normalized intensities of transcription sites over time, for the same cells as in **g**. The normalization was done according to the value measured at $t = 0$. Standard deviations are provided ($n = 14$).

Plants are sessile organisms that developed exquisitely efficient regulation systems to ensure homeostasis in the face of changing environmental conditions. Due to the fast and sensitive tuning of transcriptional mechanisms, microfluidics offers the ideal solution to control environmental conditions. This strategy could be extended to a variety of other stresses (including biotic ones) and to all plant organs, as various microfluidic systems exist to study aerial parts. The technological developments made here thus open entirely new possibilities by allowing the direct visualization of transcriptional regulation in living plants, in real time and at the level of single cells and single molecules.

Integration of single-cell responses to phosphate signalling at the tissular level. The capacity to dissect transcriptional responses of individual cells within a tissue and between different tissues within an organ is a major step forward. The use of real-time phosphate radioisotope imaging[42] revealed that P_i enters and accumulates in the root tip within less than one minute[43]. The present study thus directly links this arrival with transcriptional repression, demonstrating the close concomitance between the two phenomena. Moreover, our analysis, owing to unprecedented cellular resolution in plants, also identified the heterogeneity of transcriptional responses. We observe strikingly different responses to phosphate resupply in different tissues of the root: a cell can repress *SPX1* transcription within minutes, while its neighbour may continue transcribing unabatedly (Figs. 3b, 5c and 7). The fact that the alleles of a cell show a coordinated response indicates that this heterogeneity in repression arises mainly from extrinsic sources, as expected for regulation involving a cellular signalling pathway. Interestingly, the cell-to-cell heterogeneity of *SPX1* transcription is already visible at steady state when plants are starved from phosphate: a third of root cap cells contain *SPX1* mRNAs while not being transcriptionally active, indicating discontinuous promoter activity. This peculiar phenomenon of gene bursting is an important driver of cell heterogeneity and has already been described in animals[35], but not plants. Our analysis suggests that this phenomenon may differ greatly between cell types. Using specific cell layer markers in the future will help investigate this phenomenon more precisely and decipher putative driving mechanisms. We show here with *SPX1* that transcriptional noise in plants has both intrinsic and extrinsic components, suggesting that it arises from both stochastic promoter dynamics and cellular regulatory pathways. At steady state, in the absence of P_i, intrinsic noise seems to be dominant, while extrinsic factors seem to take over during P_i refeeding, generating heterogeneity in repression kinetics and in the extent of repression. This needs to be investigated in different organs, developmental stages, physiological statuses and environmental contexts. Because of its role in cell heterogeneity, transcriptional noise is clearly a key point in understanding how the activity of individual cells is integrated within entire tissues.

Transcription imaging in polyploid cells reveals clustering of active alleles. Endoreplication in plants has been associated with high metabolic activity or fast biomass development, which is economically important for most vegetables and fruits. Recent analysis of *Arabidopsis* illustrated the extent of this process affecting many root cells during their development and differentiation, the highest level of endoploidy (16C) being observed either in the most developed cells (epidermis hair cells) or in highly active regions associated with the distribution of nutrients (phloem companion cells)[29]. So far, endoploidy detection has used destructive techniques such as flow cytometry or histochemical staining of endocycle markers or DNA. Here, we overcame such limitations, providing the opportunity to access the kinetics of endoploidy while taking into account development, cell fate and biotic or abiotic stresses. Our results highlight the magnitude of somatic polyploidy in a root, revealing that many alleles of polyploid cells can be simultaneously transcriptionally active. We found that in the absence of phosphate, active *SPX1* alleles of polyploid cells tended to cluster together, possibly because endoreplicated chromatids generally occupy the same chromosome territory[44]. More surprisingly, our data also suggest that active *SPX1* alleles tend to coalesce together, a phenomenon reminiscent of transcriptional factories reported in animal cells[34]. In the future, it will be important to confirm the coalescence of active alleles by directly observing this phenomenon in live cells. It will also be interesting to determine whether this is related to the very high transcriptional activity of the *SPX1* gene in these conditions (one initiation event every two to four seconds) and to understand how this process occurs and whether it contributes to gene regulation. Note that these initiation rates are based on polymerase elongation speed measured in animals or yeast. They do not consider possible modifications affecting transcription elongation, pausing and termination, which are poorly described in plants despite recent advances[32,33], and will require additional experiments to account for them.

Overall, the technology presented here offers direct access to RNA polymerase II activity in live cells and could be used to study crucial plant phenomena affecting transcription (such as silencing, heterozygosity and the impact of gametophyte origin). This unprecedented spatio-temporal resolution for plant transcription therefore provides new horizons to multiple applications hitherto inaccessible in plant physiology.

Methods

Plant materials and growth conditions. Wild-type *A. thaliana* Col-0 seeds were sterilized and grown vertically on Murashige and Skoog medium diluted tenfold (MS/10) in Petri dishes supplemented with a P_i source containing either 500 µM (+P) or 13 µM (−P) KH_2PO_4 in a culture chamber under a 16-h-light/8-h-dark regime (25 °C/22 °C), as previously described[45].

For the global transcriptomic analysis, seven-day-old seedlings were germinated on a sterile nylon mesh deposited at the surface of the culture medium to facilitate the transfer between media. For the resupply experiments, plantlets were transferred from −P to +P for 30, 60 or 180 minutes. To minimize stress-related transfer, control plants in −P and +P media were also transferred for a similar period on the same media.

To get closer to microfluidic conditions and limit the stresses related to the solid media transfer, we modified the protocol for subsequent experiments (RT–qPCR analyses) by transferring the seven-day-old seedlings from agar plates to liquid MS/10 for three days. Then, −P plants were resupplied with +P solution for up to three hours before the roots were collected for RNA extraction. The transcription inhibition experiments were performed by the addition of 0.6 mM cordycepin[46]. For each condition, three independent biological replicates were analysed. Plant DNA extraction and genetic segregation analysis were performed as previously described[47].

RNA-seq library preparation and analysis (RNA-seq and RT–qPCR). The extraction of total RNA from *Arabidopsis* roots or shoots, the synthesis of RNA-seq libraries and their analysis using Illumina sequencing technology (Illumina) were performed as previously described[48]. The RT–qPCR experiments were performed as previously described[49] with the primers listed in Supplementary Table 1.

For the 7-methylgunaosine RNA immunoprecipitation (m7G-RIP) experiment, total RNA was extracted using the Monarch Total RNA Miniprep kit including DNAse treatment on a column (New England Biolabs). We then performed m7G-RIP as previously described[50] with slight modifications. We used 5 µg of total RNA as the starting material. Elution was performed using 8 M guanidium for ten minutes at 65 °C followed by RNA precipitation. As a negative control, pyrophosphatase treatment was performed on total RNA prior to m7G-RIP. Reverse transcription was then performed on the input and eluate fractions using 500 ng of RNA and oligonucleotide dT primer. PCR was then performed using primers against MS2 transgene or endogenous SPX1 using the oligonucleotides described in Supplementary Table 1.

Transgene constructs. The pSPX1::MS2×128 and pUNI1::MS2×128 constructs were built using the Golden Gate cloning technique[25]. MS2×128 stem–loops (pMK123-MS2×128–XbaI) and NOS terminator were inserted into level 0 vectors pICH41308 and pICH41421, respectively. The promoters of *SPX1* (At5G20150) and *UNICORN1* (At5g20790) were PCR amplified (1,452 base pairs[28] and 2,161 base pairs upstream of the start codon) using the oligonucleotides described in Supplementary Table 1. These sequences were introduced in level 0 vectors

(pICH41295). The level 0 modules were assembled directly into a level 2 expression vector, pICH86966.

The Ubiquitin10 promoter (At4g05320) driving eGFP expression derived from pUBN-Dest[26] was assembled with MCP contained in pDONR201 (ref. [8]) using the Gateway cloning technique (Invitrogen), creating the plasmid pUb::eGFP/MCP-NLS. This construct was excised from the Gateway vector using PmeI and SmaI (Invitrogen) and introduced in level 2 transfer DNA pSPX1::MS2×128 or pUNI1::MS2×128 vectors using PmeI restriction sites. A clone having the two constructs in opposite orientations, creating pMCP/proSPX1::MS2, was used to transform *Agrobacterium tumefaciens* strain C58C1. Supplementary Fig. 2a summarizes the cloning strategy. The reporter line carrying luciferase in fusion with the UNICORN1 promoter was generated as previously described[45].

Production of transgenic lines. Transformants produced by floral dipping[51] were selected on Hoagland/2 media complemented with 50 mg l^{-1} kanamycin. The progeny exhibiting 3:1 segregation were carried to the T3 generation to identify homozygous lines carrying a single insertion locus. At least five independent lines were obtained for each construct.

Single-molecule fluorescence in situ hybridization. *Arabidopsis* seedlings were grown on +P and −P agar media. The roots of seven- to ten-day-old seedlings were collected and fixed for 30 min with 2-(*N*-morpholino) ethane sulfonic acid (MES) buffer solution, pH 5.7, containing 4% paraformaldehyde (32% methanol-free solution; Electron Microscopy Sciences). The pH was adjusted to 5.7 with KOH solution.

Roots were rinsed twice with MES buffer (pH 5.8) and put onto a microscope slide with a coverslip. They were smoothly squashed (to splay them and produce a single cell layer) and submerged briefly in liquid nitrogen. Then, the coverslips were removed, and the samples were left out to dry at room temperature for one hour. To permeabilize the samples, the slides were immersed in 70% ethanol overnight on a rotary shaker prior to hybridization. The ethanol was evaporated at room temperature before the roots were washed with MES.

SmFISH was used for the detection of MS2 repeats and endogenous *SPX1* mRNAs. The MS2 probe was made of a mix of ten pre-labelled fluorescent oligonucleotides directed against 32×MS2 repeats[13]. Each oligonucleotide contained two to four molecules of Cy3 and hybridized four times across 128×MS2 repeats, allowing the binding of 40 probes to each single RNA molecule. The set of *SPX1* probes was made of a mix of 24 fluorescent oligonucleotides carrying two or three Cy3 fluorophores and covering the entire SPX1 transcript including the 5′ and 3′ untranslated regions (Supplementary Table 2). The pre-hybridization was performed in 1×SSC/40% formamide buffer for 15 min at room temperature. Hybridization was performed with 2 ng µl^{-1} probe and in 40% formamide for MS2, whereas for *SPX1* only 15% formamide was used. The smFISH probe mix directed against the post-poly(A) region of the MS2 construct was made of 21 oligonucleotides (Supplementary Table 2) and hybridized as previously described[52]. After the addition of the probes, the samples were covered with a coverslip and remained overnight at 37 °C as previously described[52]. For rinsing, after coverslip removal, the root samples were washed twice for 45 min at 37 °C with freshly prepared 1×SSC/40% formamide buffer, rinsed at room temperature with MES pH 5.8 buffer and dried. A drop of Prolong Diamond antifade mounting medium (Invitrogen) containing DAPI was added prior to observation. For long-term storage, the slides were kept at −20 °C.

Fluorescence imaging of fixed plants. SmFISH and MCP–GFP images were taken using either a spinning disk confocal or a wide-field microscope. For spinning disk microscopy, we used a Dragonfly (Oxford Instruments) equipped with four laser lines (405, 488, 561 and 637 nm) and an ultrasensitive EMCCD camera (iXon Life 888, Andor) mounted on a Nikon Eclipse Ti2 microscope body, using a ×40, NA 1.3 Plan Fluor oil objective or a ×60, NA 1.4 Plan Apochromat oil objective coupled with a supplementary lens of ×2, using *z*-stacks with a 0.5 µm or 0.4 µm step. For wide-field imaging, we used a Zeiss Axioimager Z1 wide-field upright microscope equipped with a camera sCMOS ZYLA 4.2 MP (Andor), using a ×100, NA 1.4 Plan Apochromat oil objective. For these *z*-stacks, a step of 0.3 or 0.4 µm was used. MIPs were generated with ImageJ v.1.53h, and the figures were realized using Adobe Photoshop 13.0.6 and Illustrator 16.0.4. The mosaic of Fig. 3a is accessible with a viewer run with Imjoy[53]. Note that plant fixation and smFISH both reduced the GFP signals.

Analysis and quantification of smFISH images. Quantification of the brightness of transcription sites was done with a modified version of HotSpot[40]. This is a user-friendly MATLAB 2020b program that allows one to quantify smFISH signals in very noisy images, unlike FISH-quant[54,55]. Briefly, the user can navigate in 2D or 3D bicolour images to manually select transcription sites and single RNAs, and the script finds the local maxima and fits 2D or 3D Gaussians to the selected transcription spots. The images of single RNAs are averaged and also fitted to 2D or 3D Gaussians, and the integrated intensities of the transcription sites are divided by the average intensity of single RNAs, yielding the exact number of molecules present at transcription sites. In this work, quantifications were done in 2D on MIPs using 100–500 single RNAs per image to generate the average. HotSpot is available on GitHub (https://github.com/muellerflorian/hotspot).

To calculate initiation rates, we assumed that initiation occurs at random with a constant rate. This produces a uniform distribution of RNA polymerases along the *SPX1* gene following an arithmetic series. Because the MS2 and *SPX1* probes are distributed homogeneously along the corresponding pre-mRNAs, incomplete nascent RNAs are labelled with only a fraction of the probes. If one assumes that the pre-mRNAs immediately leave the transcription site once polymerases reach the 3′ end of the gene (in agreement with experimental data), the barycentre of the polymerase distribution is the middle of the gene, and the average brightness of a nascent pre-mRNA is thus half that of a full-length pre-mRNA. In this case, the number of polymerases on the gene, N_{pol}, is thus twice the brightness of transcription sites, expressed in the number of full-length pre-mRNAs (noted TS_{RNA}). Assuming an elongation rate of 2 kb min^{-1}, the time to transcribe the gene, t_{el}, is 42 s, and the average initiation rate is N_{pol} divided by t_{el}. If the pre-mRNA takes t_{proc} seconds to be 3′-end processed and released from the transcription site, then N_{pol} is $TS_{RNA} \times [2 \times t_{el}/(t_{el}+t_{proc}) + t_{proc}/(t_{el}+t_{proc})]$, and the initiation rate is N_{pol} divided by $(t_{el}+t_{proc})$.

To analyse the distribution of distances separating active transcription sites within single nuclei, we computed for each nucleus all the distances between all the visible transcription sites. To simulate a random distribution of transcription sites, *Arabidopsis* nuclei were simulated as ellipses with a major axis length of 12 µm and a minor axis length of 6 µm, and we randomly selected points using a uniform distribution in the ellipse surface.

To measure total (n_{tot}), extrinsic (n_{ext}) and intrinsic (n_{int}) noise for cells with any number of alleles, we used an extension of the approaches previously developed[36,37]. For a population of cells with n alleles, we considered the brightness of the transcription sites of the n alleles, expressed in the number of full-length pre-mRNA molecules, as n random variables. We computed the corresponding variance–covariance matrix of these n variables and defined n_{tot} as the root square of the mean of the variances given by the matrix diagonal, n_{ext} as the root square of the mean of the covariances obtained by the non-diagonal values of the matrix, and n_{int} as the root square of $n_{tot}^2 - n_{ext}^2$. The error in n_{tot}, n_{int} and n_{ext} was estimated by randomly attributing each of the n transcription sites to the n alleles, calculating n_{tot}, n_{int} and n_{ext} and repeating this 100 times to calculate the standard deviation of the values obtained.

In Fig. 2d, the number of expressing cells (that is, cells having at least 20 RNA molecules in the nucleus or the cytoplasm) and the number of transcription sites per cell (Fig. 4c,d) were counted manually from 2D MIP smFISH images. The plots in Fig. 4 were generated in R v.3.2.0 and incorporated in the figure using Adobe Illustrator 16.0.4.

RootChips and in vivo live plant imaging experiments. For the live plant imaging experiments, we used the brightest lines obtained with the *SPX1* promoter (the S and J lines). Transgenic seeds were germinated in conical cylinders produced from micropipette tips filled with −P agar and inserted into sterile −P agar plates. Five- to seven-day-old P_i-deficient seedlings were then transferred into RootChips[22,38], grown vertically and fed with a P_i-deficient nutritive solution at a low flow pressure until the root grew in the channel. For the refeeding experiments, the nutritive solution was changed from $-P_i$ to $+P_i$. SynaptoRed C2 (5 µg ml^{-1}, Ozyme) was added to the +P solution to detect the arrival time of P_i (defining $t=0$). In vivo videos were recorded with an Andor Dragonfly spinning disk mounted on a Nikon Eclipse Ti using a ×40 Plan-Apo water objective (1.15 NA; 0.6 mm DT). *Z*-stacks were made every three minutes with a scan size of 100–150 µm (0.5 µm step size; ~200 steps per *z*-stack). The data were analysed with ImageJ using the TrackMate plug-in to track transcription sites on 2D MIPs. The intensity of *SPX1* transcription sites was assessed for several nuclei per sample. In each nucleus, the mean intensity of the nuclear background was subtracted from the maximum intensity of the *SPX1* transcription site, and the resulting intensities were plotted against time.

Reporting Summary. Further information on research design is available in the Nature Research Reporting Summary linked to this article.

Data availability

The genetic constructs, lines and datasets generated in the current study are available from the corresponding author upon request.

Received: 16 October 2020; Accepted: 7 July 2021;
Published online: 9 August 2021

References

1. Lopez-Maury, L., Marguerat, S. & Bahler, J. Tuning gene expression to changing environments: from rapid responses to evolutionary adaptation. *Nat. Rev. Genet.* **9**, 583–593 (2008).
2. Birnbaum, K. et al. A gene expression map of the *Arabidopsis* root. *Science* **302**, 1956–1960 (2003).
3. Balleza, E., Kim, J. M. & Cluzel, P. Systematic characterization of maturation time of fluorescent proteins in living cells. *Nat. Methods* **15**, 47–51 (2018).

4. Sorenson, R. S., Deshotel, M. J., Johnson, K., Adler, F. R. & Sieburth, L. E. *Arabidopsis* mRNA decay landscape arises from specialized RNA decay substrates, decapping-mediated feedback, and redundancy. *Proc. Natl Acad. Sci. USA* **115**, E1485–E1494 (2018).
5. Narsai, R. et al. Genome-wide analysis of mRNA decay rates and their determinants in *Arabidopsis thaliana*. *Plant Cell* **19**, 3418–3436 (2007).
6. Kollist, H. et al. Rapid responses to abiotic stress: priming the landscape for the signal transduction network. *Trends Plant Sci.* **24**, 25–37 (2019).
7. Bertrand, E. et al. Localization of ASH1 mRNA particles in living yeast. *Mol. Cell* **2**, 437–445 (1998).
8. Fusco, D. et al. Single mRNA molecules demonstrate probabilistic movement in living mammalian cells. *Curr. Biol.* **13**, 161–167 (2003).
9. Boireau, S. et al. The transcriptional cycle of HIV-1 in real-time and live cells. *J. Cell Biol.* **179**, 291–304 (2007).
10. Lucas, T. et al. Live imaging of bicoid-dependent transcription in *Drosophila* embryos. *Curr. Biol.* **23**, 2135–2139 (2013).
11. Chao, J. A., Patskovsky, Y., Almo, S. C. & Singer, R. H. Structural basis for the coevolution of a viral RNA–protein complex. *Nat. Struct. Mol. Biol.* **15**, 103–105 (2008).
12. Pichon, X., Lagha, M., Mueller, F. & Bertrand, E. A growing toolbox to image gene expression in single cells: sensitive approaches for demanding challenges. *Mol. Cell* **71**, 468–480 (2018).
13. Tantale, K. et al. A single-molecule view of transcription reveals convoys of RNA polymerases and multi-scale bursting. *Nat. Commun.* **7**, 12248 (2016).
14. Misson, J. et al. A genome-wide transcriptional analysis using *Arabidopsis thaliana* Affymetrix gene chips determined plant responses to phosphate deprivation. *Proc. Natl Acad. Sci. USA* **102**, 11934–11939 (2005).
15. Thibaud, M. C. et al. Dissection of local and systemic transcriptional responses to phosphate starvation in *Arabidopsis*. *Plant J.* **64**, 775–789 (2010).
16. Rubio, V. et al. A conserved MYB transcription factor involved in phosphate starvation signaling both in vascular plants and in unicellular algae. *Genes Dev.* **15**, 2122–2133 (2001).
17. Bustos, R. et al. A central regulatory system largely controls transcriptional activation and repression responses to phosphate starvation in *Arabidopsis*. *PLoS Genet.* **6**, e1001102 (2010).
18. Puga, M. I. et al. SPX1 is a phosphate-dependent inhibitor of PHOSPHATE STARVATION RESPONSE 1 in *Arabidopsis*. *Proc. Natl Acad. Sci. USA* **111**, 14947–14952 (2014).
19. Wang, Z. et al. Rice SPX1 and SPX2 inhibit phosphate starvation responses through interacting with PHR2 in a phosphate-dependent manner. *Proc. Natl Acad. Sci. USA* **111**, 14953–14958 (2014).
20. Zhu, J. et al. Two bifunctional inositol pyrophosphate kinases/phosphatases control plant phosphate homeostasis. *eLife* https://doi.org/10.7554/eLife.43582 (2019).
21. Wild, R. et al. Control of eukaryotic phosphate homeostasis by inositol polyphosphate sensor domains. *Science* **352**, 986–990 (2016).
22. Grossmann, G. et al. The RootChip: an integrated microfluidic chip for plant science. *Plant Cell* **12**, 4234–4240 (2011).
23. Misson, J., Thibaud, M. C., Bechtold, N., Raghothama, K. & Nussaume, L. Transcriptional regulation and functional properties of *Arabidopsis* Pht1;4, a high affinity transporter contributing greatly to phosphate uptake in phosphate deprived plants. *Plant Mol. Biol.* **55**, 727–741 (2004).
24. Tutucci, E. et al. An improved MS2 system for accurate reporting of the mRNA life cycle. *Nat. Methods* **15**, 81–89 (2018).
25. Engler, C., Gruetzner, R., Kandzia, R. & Marillonnet, S. Golden gate shuffling: a one-pot DNA shuffling method based on type IIs restriction enzymes. *PLoS ONE* **4**, e5553 (2009).
26. Grefen, C. et al. A ubiquitin-10 promoter-based vector set for fluorescent protein tagging facilitates temporal stability and native protein distribution in transient and stable expression studies. *Plant J.* **64**, 355–365 (2010).
27. Duncan, S., Olsson, T. S. G., Hartley, M., Dean, C. & Rosa, S. A method for detecting single mRNA molecules in *Arabidopsis thaliana*. *Plant Methods* **12**, 13 (2016).
28. Duan, K. et al. Characterization of a sub-family of *Arabidopsis* genes with the SPX domain reveals their diverse functions in plant tolerance to phosphorus starvation. *Plant J.* **54**, 965–975 (2008).
29. Bhosale, R. et al. A spatiotemporal DNA endoploidy map of the *Arabidopsis* root reveals roles for the endocycle in root development and stress adaptation. *Plant Cell* **30**, 2330–2351 (2018).
30. Levsky, J. M., Shenoy, S. M., Pezo, R. C. & Singer, R. H. Single-cell gene expression profiling. *Science* **297**, 836–840 (2002).
31. Femino, A. M., Fay, F. S., Fogarty, K. & Singer, R. H. Visualization of single RNA transcripts in situ. *Science* **280**, 585–590 (1998).
32. Zhu, J., Liu, M., Liu, X. & Dong, Z. RNA polymerase II activity revealed by GRO-seq and pNET-seq in *Arabidopsis*. *Nat. Plants* **4**, 1112–1123 (2018).
33. Hetzel, J., Duttke, S. H., Benner, C. & Chory, J. Nascent RNA sequencing reveals distinct features in plant transcription. *Proc. Natl Acad. Sci. USA* **113**, 12316–12321 (2016).
34. Furlong, E. E. M. & Levine, M. Developmental enhancers and chromosome topology. *Science* **361**, 1341–1345 (2018).
35. Garcia, H. G., Tikhonov, M., Lin, A. & Gregor, T. Quantitative imaging of transcription in living *Drosophila* embryos links polymerase activity to patterning. *Curr. Biol.* **23**, 2140–2145 (2013).
36. Alamos, S., Reimer, A., Niyogi, K. K. & Garcia, H. G. Quantitative imaging of RNA polymerase II activity in plants reveals the single-cell basis of tissue-wide transcriptional dynamics. *Nat. Plants* https://doi.org/10.1038/s41477-021-00976-0 (2021).
37. Elowitz, M. B., Levine, A. J., Siggia, E. D. & Swain, P. S. Stochastic gene expression in a single cell. *Science* **297**, 1183–1186 (2002).
38. Guichard, M., Bertran Garcia de Olalla, E., Stanley, C. E. & Grossmann, G. Microfluidic systems for plant root imaging. *Methods Cell. Biol.* **160**, 381–404 (2020).
39. Bayle, V. et al. *Arabidopsis thaliana* high-affinity phosphate transporters exhibit multiple levels of posttranslational regulation. *Plant Cell* **23**, 1523–1535 (2011).
40. Pichon, X. et al. Visualization of single endogenous polysomes reveals the dynamics of translation in live human cells. *J. Cell Biol.* **214**, 769–781 (2016).
41. Pena, E. J. & Heinlein, M. RNA transport during TMV cell-to-cell movement. *Front. Plant Sci.* **3**, 193 (2012).
42. Kanno, S. et al. Development of real-time radioisotope imaging systems for plant nutrient uptake studies. *Phil. Trans. R. Soc. B* **367**, 1501–1508 (2012).
43. Kanno, S. et al. A novel role for the root cap in phosphate uptake and homeostasis. *eLife* **5**, e14577 (2016).
44. Schubert, V., Berr, A. & Meister, A. Interphase chromatin organisation in *Arabidopsis* nuclei: constraints versus randomness. *Chromosoma* **121**, 369–387 (2012).
45. Hanchi, M. et al. The phosphate fast-responsive genes PECP1 and PPsPase1 affect phosphocholine and phosphoethanolamine content. *Plant Physiol.* **176**, 2943–2962 (2018).
46. Gutierrez, R. A., Ewing, R. M., Cherry, J. M. & Green, P. J. Identification of unstable transcripts in *Arabidopsis* by cDNA microarray analysis: rapid decay is associated with a group of touch- and specific clock-controlled genes. *Proc. Natl Acad. Sci. USA* **99**, 11513–11518 (2002).
47. Sarrobert, C. et al. Identification of an *Arabidopsis thaliana* mutant accumulating threonine resulting from mutation in a new dihydrodipicolinate synthase gene. *Plant J.* **24**, 357–367 (2000).
48. Secco, D. et al. Stress induced gene expression drives transient DNA methylation changes at adjacent repetitive elements. *eLife* https://doi.org/10.7554/eLife.09343 (2015).
49. Godon, C. et al. Under phosphate starvation conditions, Fe and Al trigger accumulation of the transcription factor STOP1 in the nucleus of *Arabidopsis* root cells. *Plant J.* **99**, 937–949 (2019).
50. Pandolfini, L. et al. METTL1 promotes let-7 microRNA processing via m7G methylation. *Mol. Cell* **74**, 1278–1290 (2019).
51. Harrison, S. J. et al. A rapid and robust method of identifying transformed *Arabidopsis thaliana* seedlings following floral dip transformation. *Plant Methods* **2**, 19 (2006).
52. Tsanov, N. et al. smiFISH and FISH-quant—a flexible single RNA detection approach with super-resolution capability. *Nucleic Acids Res.* **44**, e165 (2016).
53. Ouyang, W., Mueller, F., Hjelmare, M., Lundberg, E. & Zimmer, C. ImJoy: an open-source computational platform for the deep learning era. *Nat. Methods* **16**, 1199–1200 (2019).
54. Mueller, F. et al. FISH-quant: automatic counting of transcripts in 3D FISH images. *Nat. Methods* **10**, 277–278 (2013).
55. Dufrene, Y. F., Martinez-Martin, D., Medalsy, I., Alsteens, D. & Muller, D. J. Multiparametric imaging of biological systems by force-distance curve-based AFM. *Nat. Methods* **10**, 847–854 (2013).

Acknowledgements

S.H. was supported by a PhD fellowship from the CEA and PACA region, the ANR Reglisse 13-ADAP-008 fellowship and the CEA DRF impulsion programme, and the FOSSI project supported E.M., L.C., L.N., M.-C.T. and P.D. Additional grant support was received by H.J. from CEA-Enhanced Eurotalent and ANR PhlowZ 19-CE-13-0007. We thank the Heliobiotech platform for access to their RT–qPCR machine. We thank E. Basyuk for her help with the MS2 plasmids, and we thank L. Laplaze and G. Desbrosses for providing access to the growth chambers of IRD and Montpellier University. We thank O. Radulescu for his help with calculating total, extrinsic and intrinsic noise for an undefined number of alleles; T. Desnos and C. Mercier for their assistance on figure drawing; and S. Kanno and H. Garcia for critical reading of the manuscript. We thank J. Escudier for the synthesis of the SPX1 set of fluorescent probes. We acknowledge the MRI imaging facility (belonging to the National Infrastructure France-BioImaging supported by the French National Research Agency, ANR-10-INBS-04) and the ZoOM platform (supported by the Région Provence Alpes Côte d'Azur, the Conseil General of Bouches du Rhône, the French Ministry of Research, the Centre National de la Recherche Scientifique and the Commissariat à l'Energie Atomique et aux Energies Alternatives).

Author contributions

E.B. provided the MS2 and MCP original constructs, and L.N. conceived the experiments. L.C., S.H. and P.D. performed all the experiments under the supervision of L.N. for the physiological part and E.B. for cell biology. The RNA-seq data were produced by D.S. and J.W. and analysed by L.N., L.C. M.-C.T. and E.M. The luminescence experiments were performed by N.P. under the supervision of H.J. H.J. also implemented the microfluidic technique in the SAVE team. R.M. performed the experiments for cap and polyA tail detection, F.M. provided assistance for image analysis and computation and O.F. took part in the spinning disk and mosaic acquisition experiments. The manuscript was written by L.N. and E.B. with help from S.H., P.D. and L.C.

Competing interests

The authors declare no competing interests.

Additional information

Supplementary information The online version contains supplementary material available at https://doi.org/10.1038/s41477-021-00981-3.

Correspondence and requests for materials should be addressed to E.B. or L.N.

Peer review information *Nature Plants* thanks Zhicheng Dong and the other, anonymous, reviewer(s) for their contribution to the peer review of this work.

Reprints and permissions information is available at www.nature.com/reprints.

Publisher's note Springer Nature remains neutral with regard to jurisdictional claims in published maps and institutional affiliations.

nature research

Corresponding author(s): Nussaume Laurent

Last updated by author(s): 01_07_2021

Reporting Summary

Nature Research wishes to improve the reproducibility of the work that we publish. This form provides structure for consistency and transparency in reporting. For further information on Nature Research policies, see our Editorial Policies and the Editorial Policy Checklist.

Statistics

For all statistical analyses, confirm that the following items are present in the figure legend, table legend, main text, or Methods section.

n/a	Confirmed	
☐	☒	The exact sample size (*n*) for each experimental group/condition, given as a discrete number and unit of measurement
☐	☒	A statement on whether measurements were taken from distinct samples or whether the same sample was measured repeatedly
☐	☒	The statistical test(s) used AND whether they are one- or two-sided *Only common tests should be described solely by name; describe more complex techniques in the Methods section.*
☐	☒	A description of all covariates tested
☒	☐	A description of any assumptions or corrections, such as tests of normality and adjustment for multiple comparisons
☐	☒	A full description of the statistical parameters including central tendency (e.g. means) or other basic estimates (e.g. regression coefficient) AND variation (e.g. standard deviation) or associated estimates of uncertainty (e.g. confidence intervals)
☐	☒	For null hypothesis testing, the test statistic (e.g. *F*, *t*, *r*) with confidence intervals, effect sizes, degrees of freedom and *P* value noted *Give P values as exact values whenever suitable.*
☒	☐	For Bayesian analysis, information on the choice of priors and Markov chain Monte Carlo settings
☒	☐	For hierarchical and complex designs, identification of the appropriate level for tests and full reporting of outcomes
☒	☐	Estimates of effect sizes (e.g. Cohen's *d*, Pearson's *r*), indicating how they were calculated

Our web collection on statistics for biologists contains articles on many of the points above.

Software and code

Policy information about availability of computer code

Data collection	For getting maximal image projection to analyze SmFish produced by spinning disk imaginging we used free ImageJ software. For qPCR datawe used light cycler 480 software 1.5.0 (Roche). For Luminescence data were collected with ANDOR Solis software We have also used excel software to collect many quantitative data.
Data analysis	For molecular analysis (qPCR) we also used light cycler 480 software 1.5.0 (Roche) and for statistical treatment we used a free open source tool (RStudio). Then for analysing and quantify transcription on these images we used a modified version of HotSpot, a user-friendly MatLab software. Materials provide full description of calculation and link to get HotSpot. For in vivo live plant imaging analysis we analyzed transcription site using Image J software with the TrackMate plug-in. FISH-quant (Mueller et al., 2013. Nature methods 10, 277-27) was used for control requested by reviewers (introduced in rebutal letter only)

For manuscripts utilizing custom algorithms or software that are central to the research but not yet described in published literature, software must be made available to editors and reviewers. We strongly encourage code deposition in a community repository (e.g. GitHub). See the Nature Research guidelines for submitting code & software for further information.

Data

Policy information about availability of data

All manuscripts must include a data availability statement. This statement should provide the following information, where applicable:

- Accession codes, unique identifiers, or web links for publicly available datasets
- A list of figures that have associated raw data
- A description of any restrictions on data availability

-Accession code and unique identifiers are provided for all genes analyzed in this study
We do not have any restrictions on data availability and will provide on request any material of this study.

Field-specific reporting

Please select the one below that is the best fit for your research. If you are not sure, read the appropriate sections before making your selection.

☒ Life sciences ☐ Behavioural & social sciences ☐ Ecological, evolutionary & environmental sciences

For a reference copy of the document with all sections, see nature.com/documents/nr-reporting-summary-flat.pdf

Life sciences study design

All studies must disclose on these points even when the disclosure is negative.

Sample size	Most sample size were calculated to collect enough materials requested for performing experiments. With current molecular biology techniques on average for a single experiments we performent 3 technical replicates (using around 20 plantlets for each of them). For Fish experiments we analyzed for each condition 15 to 20 plantlets. For live imaging we analyze 5 plants.
Data exclusions	No data exclusion
Replication	All molecular biology experiments were at least performed using three independant biological replicates. For each values obtained requesting quantification (qPCR) we also performed technical replicates (three for all qPCR provided in molecular analysis). In situ were replicated at least three time independantly
Randomization	The main randomization is performed during plant growth requesting at least 3 Petri dishes (containing each 20 plantlets) under different Pi regime which are randomized in the growth chamber to avoid position effect.
Blinding	Blinding was not requested as we mostly tested effect of ion addition versus non treated control. Statistical test (SNK one way ANOVA was used to confirm significance of the experiments performed).

Reporting for specific materials, systems and methods

We require information from authors about some types of materials, experimental systems and methods used in many studies. Here, indicate whether each material, system or method listed is relevant to your study. If you are not sure if a list item applies to your research, read the appropriate section before selecting a response.

Materials & experimental systems

n/a	Involved in the study
☒	☐ Antibodies
☒	☐ Eukaryotic cell lines
☒	☐ Palaeontology and archaeology
☒	☐ Animals and other organisms
☒	☐ Human research participants
☒	☐ Clinical data
☒	☐ Dual use research of concern

Methods

n/a	Involved in the study
☒	☐ ChIP-seq
☒	☐ Flow cytometry
☒	☐ MRI-based neuroimaging